Supplemental Information

Evolving precision: rRNA Expansion Segment 7S modulates translation velocity and accuracy in eukaryal ribosomes

Robert Rauscher[1], Cristian Eggers[1,2], Lyudmila Dimitrova-Paternoga[3], Vaishnavi Shankar[1,2], Alessia Rosina[1,2], Marina Cristodero[1], Helge Paternoga[3], Daniel N. Wilson[3], Sebastian A. Leidel[1], Norbert Polacek[1,4,*]

[1] Department for Chemistry, Biochemistry and Pharmaceutical Sciences, University of Bern, Freiestrasse 3, 3012 Bern, Switzerland

[2] Graduate School for Cellular and Biomedical Sciences, University of Bern, Bern, Switzerland

[3] Institute for Biochemistry and Molecular Biology, University of Hamburg, Martin-Luther-King-Platz 6, 20146 Hamburg, Germany

[4]Lead contact

*Correspondence: Tel: +41 31 684 43 20; e-mail: norbert.polacek@unibe.ch

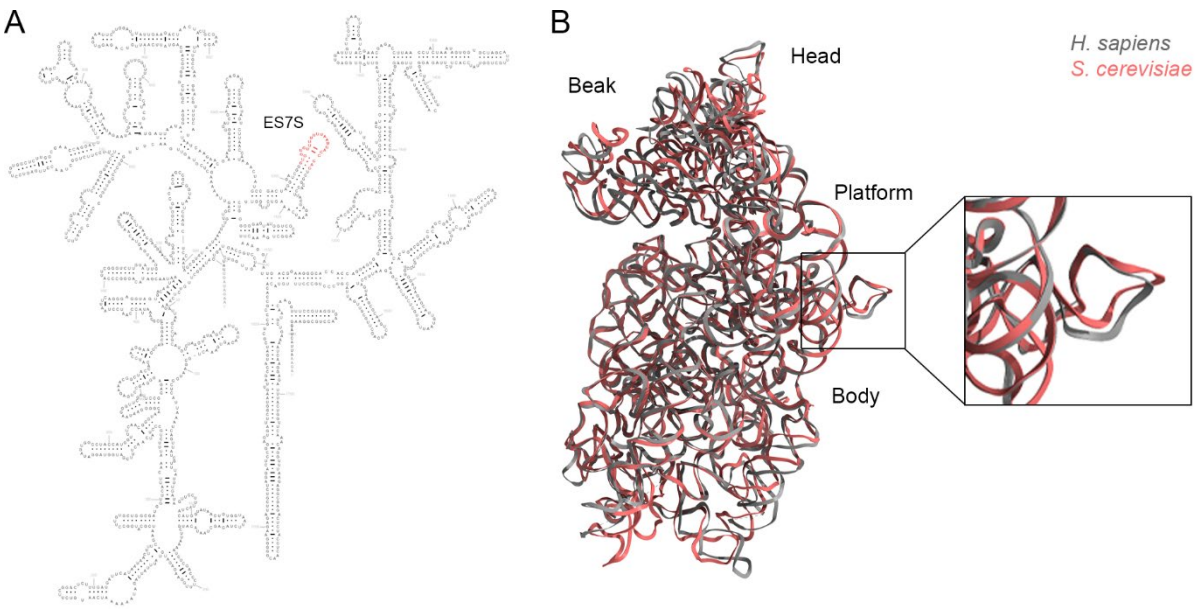

Figure S1: ES7S in human and yeast 18S rRNA acquires an identical structure

(A) The yeast 18S rRNA secondary structure is shown and ES7S is highlighted in salmon. The structure was retrieved from RNAcentral (Petrov et al., 2017a). (B) Human (5aj0) and yeast (4v88) ribosomal structures were downloaded from the protein database and 18S rRNA was aligned using the ChimeraX software(Goddard et al., 2018). Structural regions of the small subunit are indicated. ES7S is highlighted in the box.

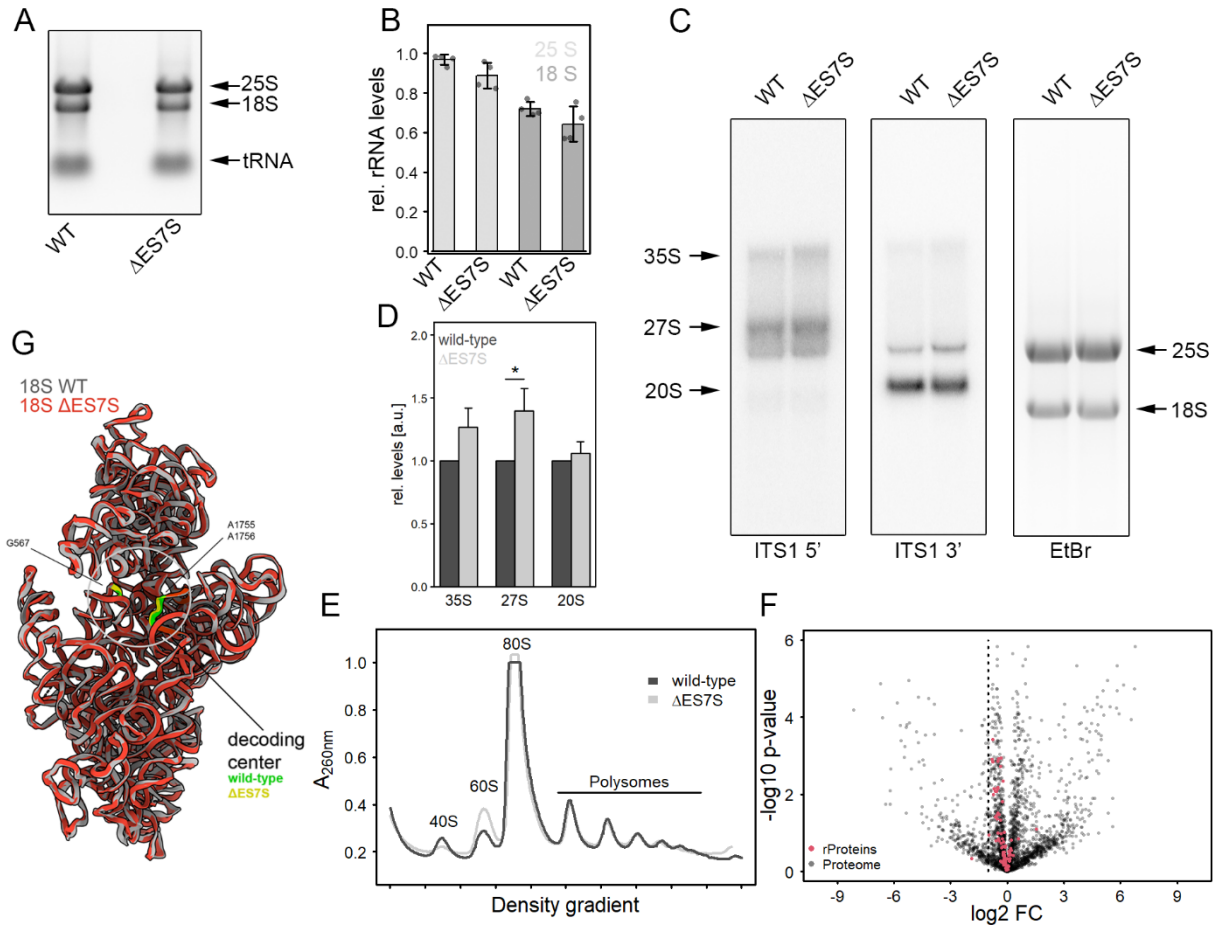

Figure S2: ΔES7S does not alter ribosomal levels and biogenesis

(A) Total RNA from equal OD_{600} units of cells were isolated and RNA electrophoresed in agarose gels. (B) Band intensities were quantified and normalized to tRNA levels. (C) Total RNA was blotted on a nylon membrane and precursors were detected by northern blot against the ITS1 before or after the A2 processing step (Krauer et al., 2021). Bands were quantified, normalized to EtBr signals and ΔES7S over wild-type ratios were calculated (D) Stars indicate significant differences ($p \leq 0.05$, $n = 4$). (E) Polysomes were extracted from cells at $OD_{600} = 0.8$ and separated by density-gradient centrifugation. Positions of free subunits, the 80S monosome and the polysomes are indicated. (F) protein levels in ΔES7S and wild-type cells were compared by mass spectrometry and quantified using the MaxQuant algorithm (Cox et al., 2014). The proteomic changes are depicted in grey and ribosomal proteins are highlighted in red. (G) 18S rRNA three-dimensional structure was solved using cryo-electron microscopy. The truncated structure was overlayed with the wild-type structure (pdb: 4U50). Crucial residues of the decoding center are highlighted in yellow (ΔES7S) and green (wild-type).

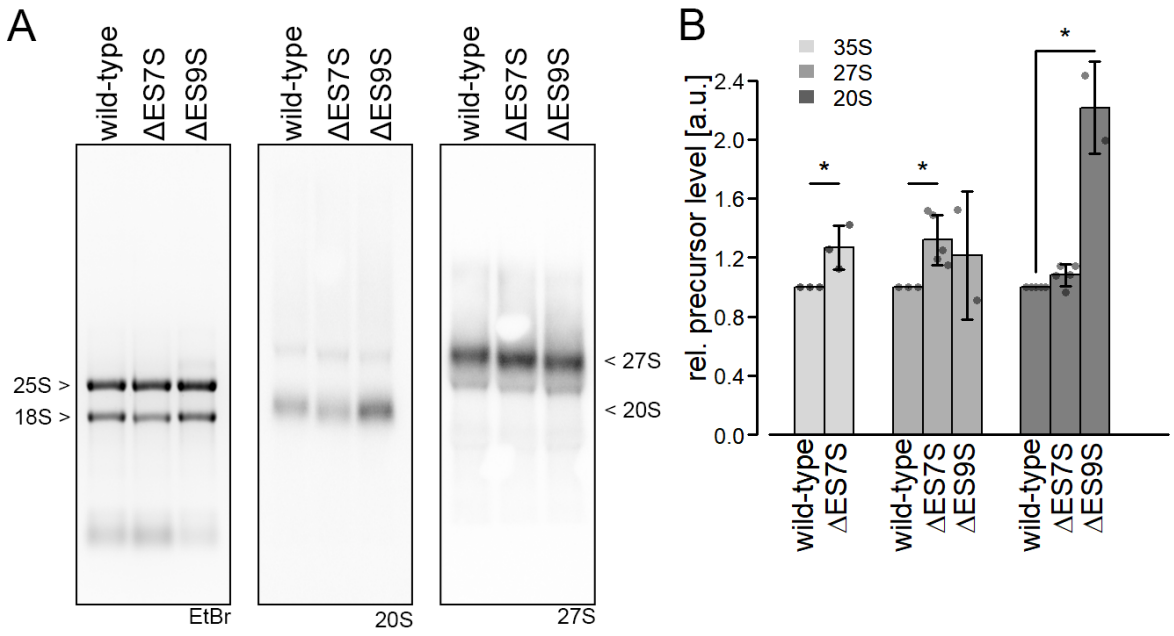

Figure S3: ES9S ablation causes biogenesis defect within the small subunit

(A) Total RNA was blotted on a nylon membrane and precursors were detected by northern blot against the ITS1 before or after the A2 processing step (Krauer et al., 2021). Bands were quantified, normalized to EtBr signals and ΔES7S over wild-type ratios were calculated (B) Stars indicate significant differences ($p \leq 0.05$, n = 2-5)

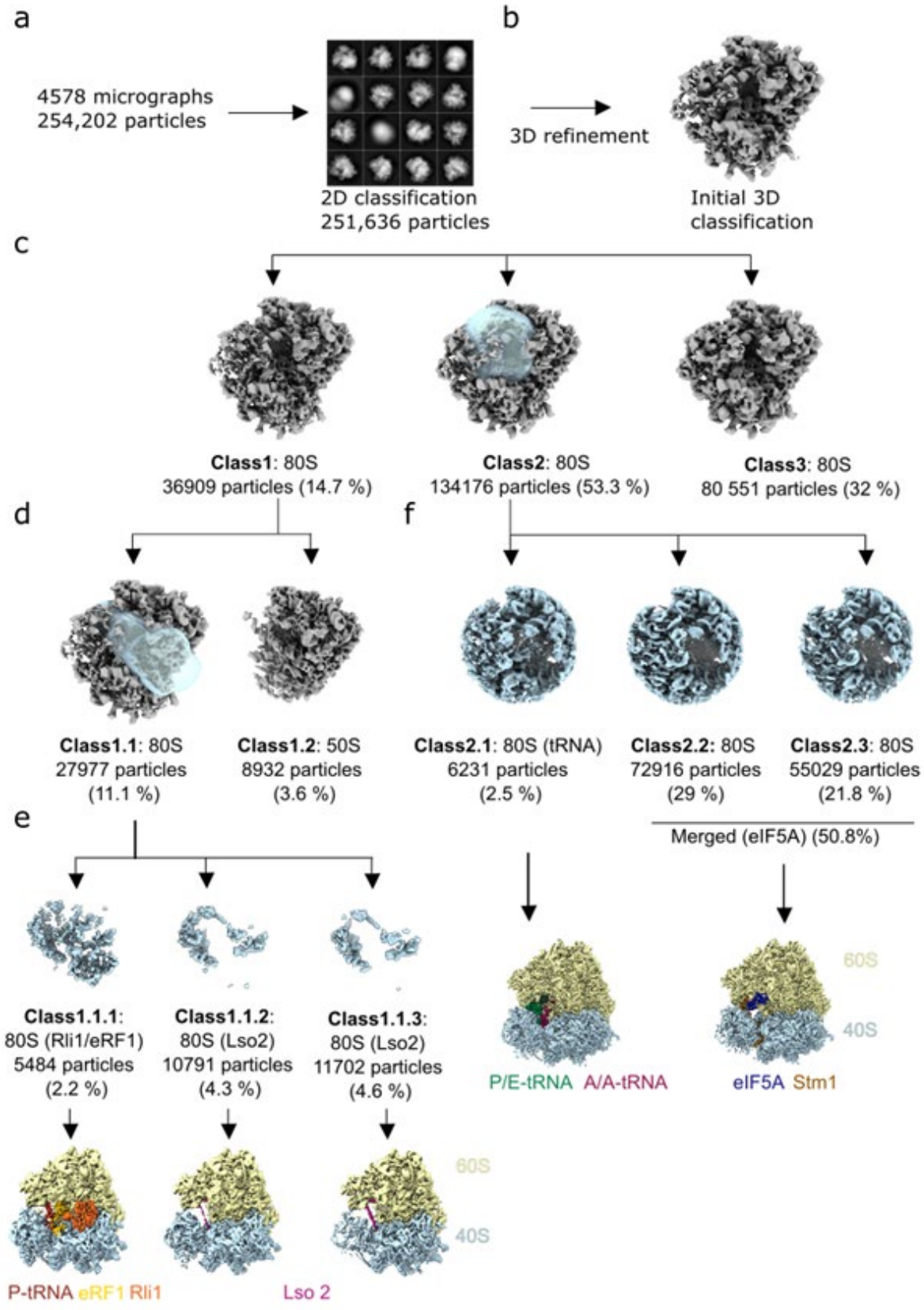

Figure S4: In silico sorting of the cryo-EM data for the yeast 80S-ES7SΔ ribosomes

(A) 254,202 particles were picked from 4,578 micrographs and 2D classified, from which (B) 251,636 particles were selected and 3D refined using a yeast wildtype 80S ribosome (PDB ID 4U50)(Garreau De Loubresse et al., 2014) as a reference. (C) The unmasked 3D classification was performed, yielding three different 80S classes, which were

sub-sorted further. (D) Unmasked classification for class 1 yielded two subclasses, class 1.1 containing 80S ribosomes (11%) and class 1.2 containing 60S subunits (3.6%). (E) Three minor populations were observed, one with dormant ribosomes bound with Lso2, a second with terminating/recycling ribosomes in complex with P-site tRNA, eRF1 and Rli1, and a third containing two tRNAs and thus constituting the actively translating ribosomes. Class 1.1, which had a density around the E site, was subtracted with a mask around the A, P and E sites and 3D was classified into three further subclasses, one containing ABCE and eRF1 (Class 1.1.1), and two containing Lso1 in different states (Classes 1.1.2 and 1.1.3). (F) The second initial 3D class (class 2) was subtracted using a mask around the E site and 3D classified into three further subclasses, one containing A/A- and P/E-tRNAs in rotated state (class 2.1), and two classes with eIF5A bound in the E-site (classes 2.2 and 2.3). The two eIF5A subclasses were near-identical and therefore merged for further analysis. The two maps were postprocessed, CTF-refined and Bayesian polished, yielding final maps with overall resolutions of 3.1 Å (tRNA class) and 2.4 Å (eIF5A class), respectively, which enabled the identification of the molecular details for how the hyposine moiety of eIF5A interacts with the ribosome, and also led to the identification of an additional binding site for ribosomal protein eL41.

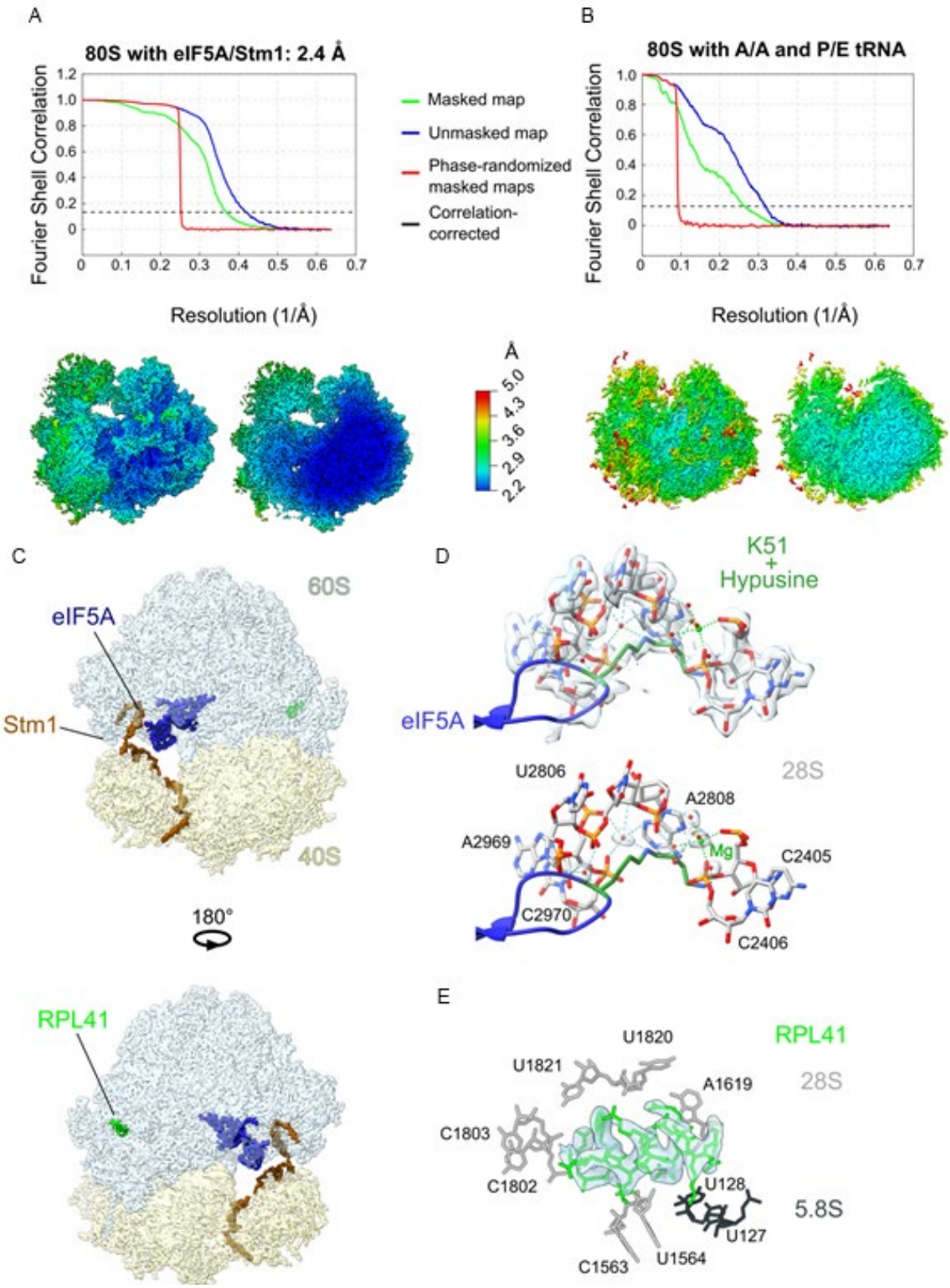

Figure S5: Cryo-EM data processing of the eIF5A/Stm1 ribosome complexes

(A-B) Fourier Shell Correlation (FSC) curves of the (A) postprocessed 80S-eIF5A/Stm1 complex and (B) the A/A- and P/E-tRNA complex. The dashed line at 0.143 indicates an average resolution of 2.4 Å and 3.1 Å for (a) and (b), respectively. Beneath the respective FSC curves are overviews (left) and transverse sections (right) of the cryo-EM maps colored in accordance to local resolution. (C) Two views of the hibernating 80S-ES7SΔ ribosome with eIF5A (blue), Stm1 (brown) and RPL41 (green) highlighted. (D) Interaction network of the hypusinated lysine 51 (K51,

dark green) of eIF5A (blue) with 28S rRNA (grey), mediated by water molecules (red) and a putative Mg2+ ion (light green). The upper panel includes density (grey transparent) for the hypsine and 28S rRNA and the lower panel includes density for the waters and Mg ion. (E) Interactions of the second copy of RPL41 (green) with 28S rRNA (grey) and 5.8S rRNA (anthracite). In (E), the density shown as grey transparency is shown for RPL41.

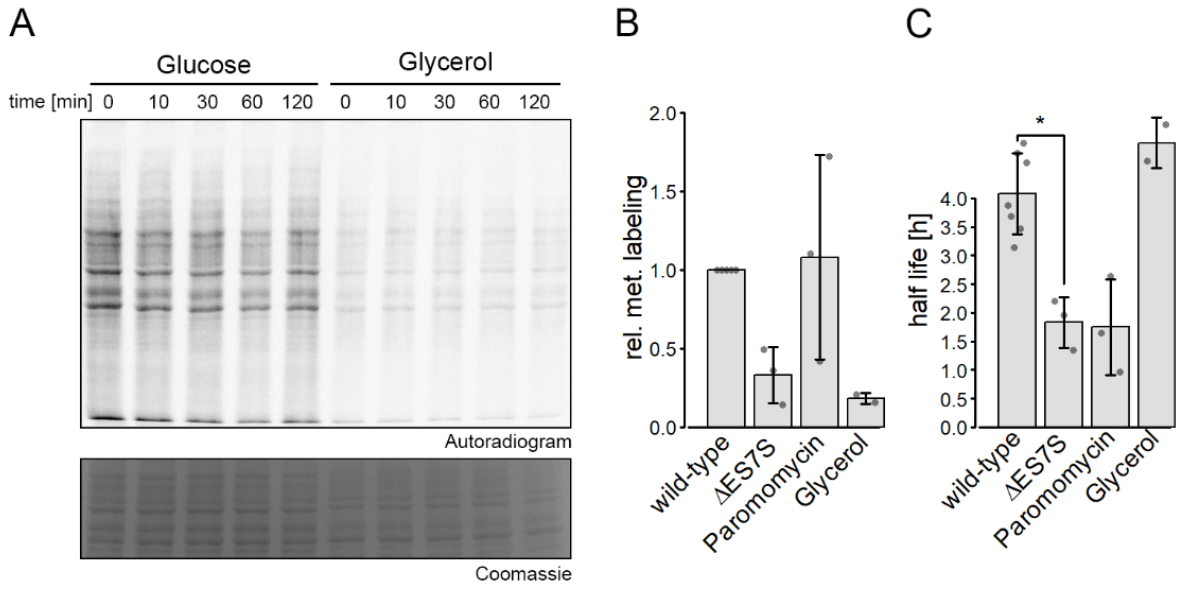

Figure S6: Protein stability in slow growth conditions

(A) Wild-type cells were grown in YP-Glucose or YP-Glycerol for 24 h and pulse/chase experiments were performed. Total labeled protein was separated in a 10% SDS PAGE, stained and exposed. (B) Initial labeling intensity after 10 min of Pulse was quantified for all pulse/chase experiments. Data are shown normalized to the wild-type as mean±SD. Individual points indicate separate data points. (C) Proteome-wide half-lifes were calculated based on the radioactive signal in A and plotted as mean±SD. Individual points indicate separate data points. Stars indicate significant differences ($p \leq 0.05$, n = 3-6)

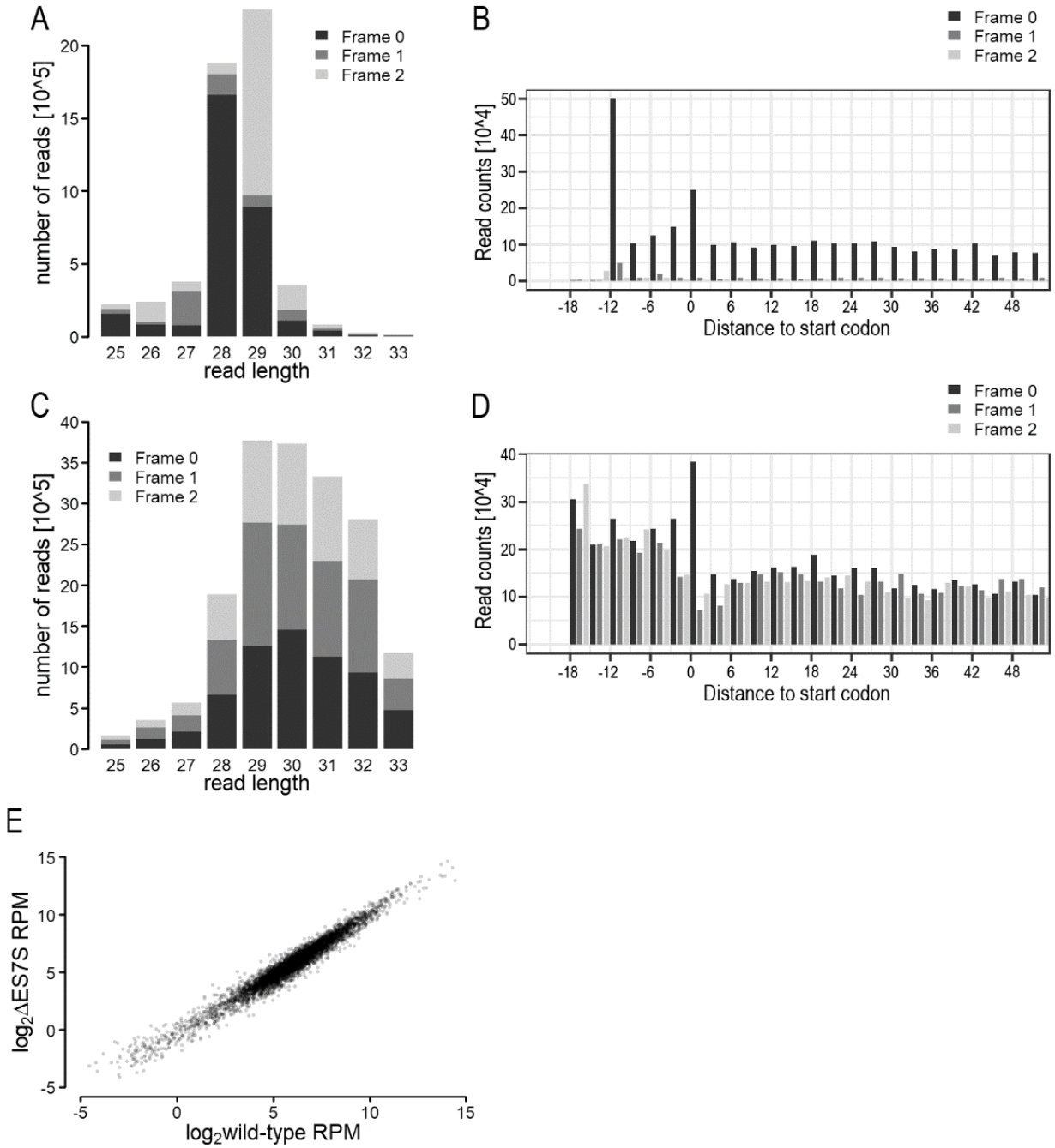

Figure S7: Ribosome profiling libraries display 3 nt periodicity

(A-B) Ribosome profiling and (C-D) mRNA Seq libraries were stratified in regard of their read length (A,C) and reading frame (B,D). Frames within one read length were binned in A and C. The metagene analysis in B and D displays the 5'-terminal position of reads in an area covering the start codon. (E) mSeq quantification of transcripts in wild-type and DES7S cells. Counts per gene were normalized to the library size (RPM) and $\log_2$ values are displayed.

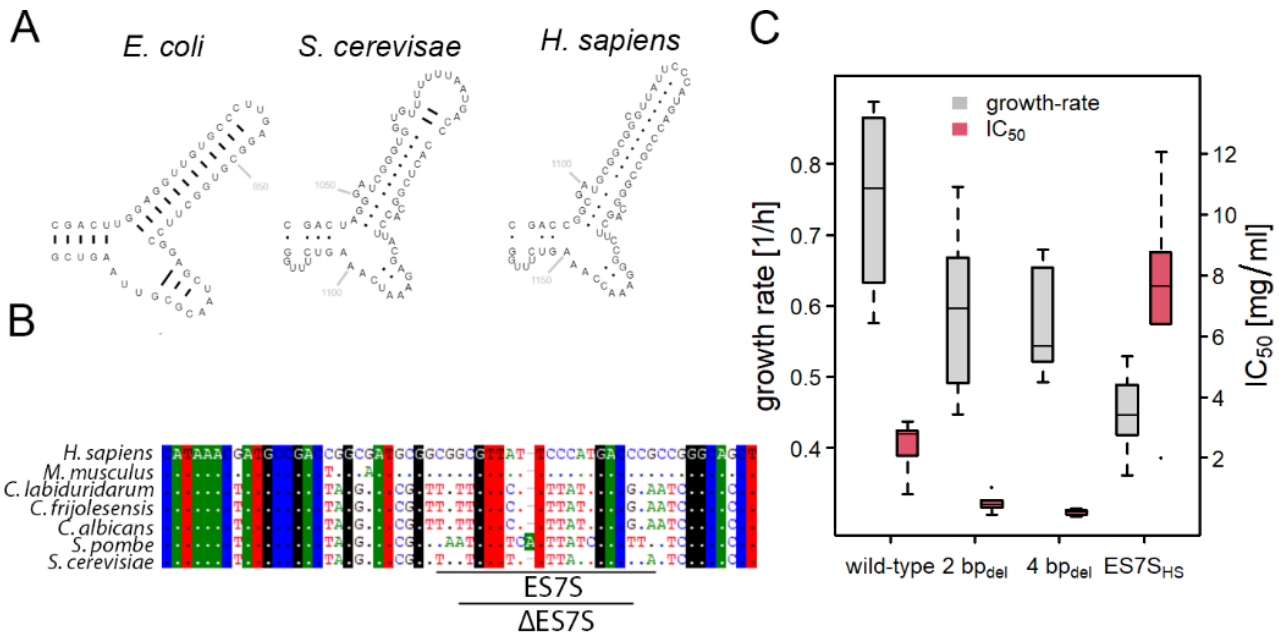

Figure S8: ES7S sequence determines susceptibility to paromomycin

(A) Secondary rRNA structure of bacterial helix 26 and mouse or human ES7S visualized using RiboVision (Bernier et al., 2014; Petrov et al., 2017b). (B) Multiple sequence alignment of *S. cerevisiae*; three related yeast strains, mouse and human 18S rRNA regions covering ES7S. Positions of ES7S and the full-length deletion are indicated. (C) *S. cerevisiae* strains carrying specific alterations of ES7S were created and growth rates and Paromomycin IC_{50} were measured (n = 5).

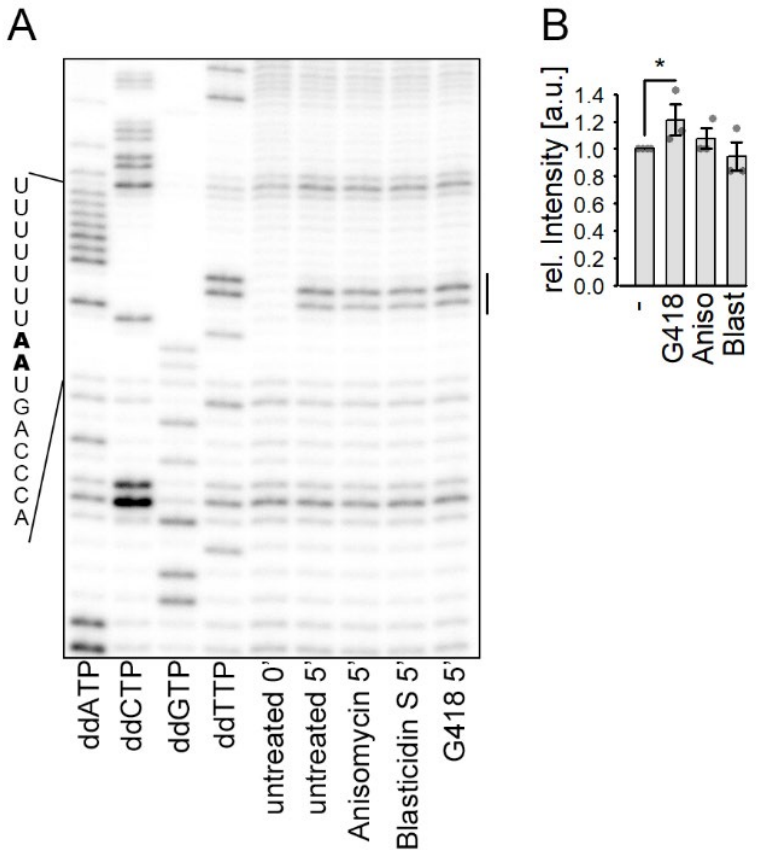

Figure S9: Antibiotics alter ES7S dynamics

Cells were treated with 84 mM DMS for 5 min and total RNA isolated. RT assays were performed to test the dynamics of ES7S (A-B). Lines indicate the adenosines within the ES7S. Signal intensity was quantified and normalized to that of untreated cells. Differences were tested for significance using Student's t-test and * indicates significant changes ($n = 3$, $p \leq 0.05$).

Table S1. Cryo-EM data collection, modelling and refinement statistics.

	80S ribosomes with eIF5A and Stm1
EMDB ID	EMD-16127
PDB ID	8BN3
Data collection	
Magnification (×)	165.000
Electron fluence (e^{-}/Å^2)	32
Defocus range (μm)	- 0.6 – 1.8 um
Pixel size (Å)	0.783
Initial particles	254 202
Final particles	127 945
Average resolution (Å) (FSC threshold 0.143)	2.4
Model composition	
Atoms	201 671
Protein residues	11 271
RNA bases	5 159
Refinement	
Map CC around atoms	0.73
Map CC whole unit cell	0.60
Map sharpening B factor (Å^2)	- 39.66
R.M.S. deviations	
Bond lengths (Å)	0.009
Bond angles (°)	1.877
Validation	
MolProbity score	1.54
Clash score	0.95
Poor rotamers (%)	2.8
Ramachandran statistics	
Favoured (%)	93.82
Outlier (%)	1.04

Supplementary References

Bernier, C. R., Petrov, A. S., Waterbury, C. C., Jett, J., Li, F., Freil, L. E., Xiong, X., Wang, L., Migliozzi, B. L. R., Hershkovits, E., Xue, Y., Hsiao, C., Bowman, J. C., Harvey, S. C., Grover, M. A., Wartell, Z. J., & Williams, L. D. (2014). RiboVision suite for visualization and analysis of ribosomes. *Faraday Discussions*, *169*(0), 195–207. https://doi.org/10.1039/C3FD00126A

Chan, P. P., & Lowe, T. M. (2016). GtRNAdb 2.0: an expanded database of transfer RNA genes identified in complete and draft genomes. *Nucleic Acids Research*, *44*(D1), D184–D189. https://doi.org/10.1093/NAR/GKV1309

Cox, J., Hein, M. Y., Luber, C. A., Paron, I., Nagaraj, N., & Mann, M. (2014). Accurate proteome-wide label-free quantification by delayed normalization and maximal peptide ratio extraction, termed MaxLFQ. *Molecular & Cellular Proteomics : MCP*, *13*(9), 2513–2526. https://doi.org/10.1074/mcp.M113.031591

Goddard, T. D., Huang, C. C., Meng, E. C., Pettersen, E. F., Couch, G. S., Morris, J. H., & Ferrin, T. E. (2018). UCSF ChimeraX: Meeting modern challenges in visualization and analysis. *Protein Science*, *27*(1), 14–25. https://doi.org/10.1002/PRO.3235

Krauer, N., Rauscher, R., & Polacek, N. (2021). tRNA Synthetases Are Recruited to Yeast Ribosomes by rRNA Expansion Segment 7L but Do Not Require Association for Functionality. *Non-Coding RNA 2021, Vol. 7, Page 73*, *7*(4), 73. https://doi.org/10.3390/NCRNA7040073

Nedialkova, D. D., & Leidel, S. A. (2015). Optimization of Codon Translation Rates via tRNA Modifications Maintains Proteome Integrity. *Cell*, *161*(7), 1606–1618. https://doi.org/10.1016/J.CELL.2015.05.022

Petrov, A. I., Kay, S. J. E., Kalvari, I., Howe, K. L., Gray, K. A., Bruford, E. A., Kersey, P. J., Cochrane, G., Finn, R. D., Bateman, A., Kozomara, A., Griffiths-Jones, S., Frankish, A., Zwieb, C. W., Lau, B. Y., Williams, K. P., Chan, P. P., Lowe, T. M., Cannone, J. J., … Dinger, M. E. (2017a). RNAcentral: a comprehensive database of non-coding RNA sequences. *Nucleic Acids Research*, *45*(Database issue), D128. https://doi.org/10.1093/NAR/GKW1008

Petrov, A. I., Kay, S. J. E., Kalvari, I., Howe, K. L., Gray, K. A., Bruford, E. A., Kersey, P. J., Cochrane, G., Finn, R. D., Bateman, A., Kozomara, A., Griffiths-Jones, S., Frankish, A., Zwieb, C. W., Lau, B. Y., Williams, K. P., Chan, P. P., Lowe, T. M., Cannone, J. J., … Dinger, M. E. (2017b). RNAcentral: a comprehensive database of non-coding RNA sequences. *Nucleic Acids Research*, *45*(Database issue), D128. https://doi.org/10.1093/NAR/GKW1008